NUMERICAL SIMULATION OF MIXED CONVECTION IN AN L-SHAPED ENCLOSURE

Nassim M. Sahraoui[1][0009-0008-9681-4047], Samir Houat[1][0000-0002-2029-5796], Abdelmalek Noureddine[1]
[1]MSMPT Group, MNEPM Laboratory, Mechanical engineering Department, FST,
Abdelhamid Ibn Badis University of Mostaganem, Mostaganem, 27000 Algeria
Email: Nassimmahfoud.Sahraoui@univ-mosta.dz

Abstract - The present study focuses on Prandtl number and Richardson number effect on mixed convection in a lid-driven L-shaped enclosure. The physical model is a two-dimensional L-shaped cavity where the bottom and left walls are maintained at a hot temperature, a cold temperature is imposed at the upper-right sides and the upper wall of the enclosure. The top wall of the cavity moves with a constant velocity at a cold temperature, whereas the right wall is insulated. The governing equations are discretized using the finite volume method (FVM). The SIMPLE algorithm is employed to couple velocity and pressure fields via the CFD software Ansys Fluent. The numerical results show very good agreement with those of the literature. The effects of different governing parameters such as Reynolds number (50 < Re < 200), Richardson number (0.1< Ri<10), and Prandtl number (0.1 < Pr < 10) on the flow and temperature fields are studied. The results indicate that the average Nusselt number grows when Richardson and Re increase. Moreover, the average Nusselt number increases as Pr and Ri increase for a fixed value of Re.

Keywords: L-shaped enclosure, Mixed convection, Finite volume method, Richardson effect, Prandtl effect.

1. Introduction

Mixed convection flows are widely involved in various industrial systems and many transport processes in nature [1-3]. It is motivated by its several applications such as heat exchangers [4-6], chemical and nuclear reactors [7,8], food and process industries [9,10] thermal energy systems [11,13], solar collectors [14], and so on, where a heat generation process takes place continuously. Mixed convection in cavities has gained recent research interest as a means of heat transfer enhancement. For instance, Sharif [15] studied mixed convection in a shallow cavity for various Richardson numbers and inclination angles ranging from 0–30◦ . He found that the average Nusselt number increases by increasing cavity inclination. Iwatsu et al [16] did a numerical study of mixed convection in a driven cavity with a stable vertical temperature gradient. They found that the heat transfer intensifies with the increase of Richardson number. Sivakumar and Sivasankaran [17] did a computational investigation of mixed convection in an inclined lid-driven square enclosure. They noticed a substantial increase in the heat transfer rate in the cavity while increasing the inclination angle. A Lattice Boltzmann method (LBM) simulation of mixed convection and radiation in a lid-driven cavity heated by a sinusoidal temperature profile was done by Dahani et al [18]. They noticed an improvement in Nusselt number when *Ri* < 1 for a given value of *Re* in the presence of radiation, while for the case of Ri > 10, heat transfer is negatively affected by the increase of Ri. A numerical study of mixed convection in a rectangular cavity using the finite difference method (FDM) was done by Papanicolaou et al [19]. The authors covered a range of Ri (0 < *Ri* < 10), and Re (50 < *Re* < 2000). They observed an increase in heat transfer when increasing *Ri* at a fixed *Re* and when increasing *Re* at a fixed *Ri.* They also found that for higher values of *Ri*, the numerical results tend to show an oscillatory behavior. Basak et al [20] did a numerical investigation to study the influence of linearly heated side walls on mixed convection flow in a square cavity. They found that average Nusselt numbers at the right and bottom walls are strongly dependent on *Gr* at larger Prandtl numbers, while for a specific value of *Pr,* the latter is a weak function of *Gr*. Islam et al [21] did a numerical study of mixed convection flow in a lid-driven cavity with an isothermal block. According to the findings, the heat

© 2025 The Author(s). Published by Cefin Publishing House – Bucharest, https://ijomam.com/
Copyright: © 2025 by the authors. Licensee IJOMAM, Romania This article is an open access article distributed under the terms and conditions of the Creative Commons. Attribution (CC BY) license (https://creativecommons.org/licenses/by/4.0/)
https://doi.org/10.17683/ijomam/issue22.v2.11

transfer increases for any size of the block when Ri>1, whilst it remains constant when Ri<1. Moreover, the optimum Nusselt number value is obtained when the block is placed at the top left and bottom right of the cavity. Mixed convection in a cavity with a heated source mounted on the bottom wall with several openings was studied by Ajmera & Mathur [22]. Their study elucidated that an increase in Ri or Re leads to an increase in the intensity of recirculation and the average Nusselt number. Mohamed et al [23] did a numerical simulation of mixed convection in a heated lid-driven cavity containing low Prandtl number fluids. They observed a stabilization of the flow for the forced convection-dominated region ($Ri < 1$) due to inertia, whilst the latter does not affect the flow for the buoyancy-dominated region (Ri > 1). Ruiz [24] did both a numerical and experimental study of natural convection in an L-Shaped and a V-shaped corners. He used water as a working fluid. He observed that the Nusselt number is higher for the horizontal wall of the L-shaped cavity compared to the vertical one. Mahmoodi [25] studied natural convection in an L-shaped enclosure. He studied the effect of the aspect ratio of the enclosure and *Ra* on the heat transfer. The author found that, for all aspect ratios, increasing *Ra* leads to an enhancement in heat transfer inside the cavity. Moreover, it was found that an increase in aspect ratio decrements the average Nusselt number. Natural convection in a L-shaped cavity was studied by Kalteh and Hasam [26]. He observed a strong relationship between Ra number and heat transfer. Shahid et al [27] did a numerical investigation of natural convection inside an L-shaped cavity using the lattice Boltzmann method. They found that the rate of natural convection increases with the increase of Rayleigh number. Mohammadifar et al. [28] did a numerical investigation of laminar natural convection of Cu/water nanofluid flow in an L-shaped cavity with an open end. The influence of Rayleigh number and aspect ratio on fluid flow and heat transfer were examined using multiple boundary conditions at the right side of the open-end cavity. The highest heat transfer improvement was reached when the imposed boundary conditions were an open end instead of fixed adiabatic. Armaghani et al. [29] studied the impact of the heat source position and size on an L-shaped enclosure having MHD mixed convection and filled with Al2O3-Cu/Water hybrid nanofluid. The authors found that the optimum heat transfer was reached using the highest sink power. LBM was used by Nia et al. [30] to study the influence of different baffle lengths and locations on the natural convection of Cu-water nanofluid heat transfer and fluid flow inside an L-shaped enclosure for different Rayleigh numbers and solid volume fractions. They found that, at lower Rayleigh number values, the addition of a baffle improves natural convection.

On the other hand, the longer baffle, despite its location, can improve natural convection for higher Rayleigh numbers. Tasnim et al [31] numerically studied free convection inside an inclined L-shaped cavity. The effects of different parameters such as *Ra* ($10^3 \leq Ra \leq 10^5$), inclination angle ($0 < \theta < 360°$) and *AR* ($0.2 < AR < 0.6$) on the flow were studied. They found that *Ra* and the inclination angle had a significant influence on the average Nusselt number, particularly in the convection-dominated zone. Ahmed et al [32] did a numerical simulation of mixed convection in a double lid-driven L-shaped enclosure with heated corners. They noticed a strong increase in the isothermal distributions when increasing the length of the heated corners. Moreover, increasing *Ri* leads to a heat transfer enhancement. Sourtiji et al [33] performed a numerical simulation of MHD natural convection in an L-shaped enclosure using nanofluids. They noticed the appearance of a clockwise vortex for lower values of *Ra*. Additionally, increasing *Ra* increases heat transfer in the enclosure. Zhang et al [34] did both numerical and experimental work to study free convection in a finned L-shaped cavity using nanofluid. Their results showed that increasing *Ra* and nanofluid volume fraction leads to an increase in the average Nusselt number. They concluded that the arrangement of fins impacted flow structures considerably. Selimefendigil and Oztop [35] did an MHD simulation of mixed convection nanofluid flow in a flexible walled inclined lid-driven L-shaped enclosure under the effect of internal heat generation. Their findings showed that the average Nusselt number increases with the decrease of *Ra* and the increase of *Ri* for the case of the rigid wall. A finite elements simulation of unsteady mixed convection of nanofluids inside a porous lid-driven L-shaped enclosure was performed by Yeasmin et al [36]. They found that *Ri* is the most influential factor that affects the flow structures and that higher values of *Re* improve drastically heat transfer rate and have a minor effect on fluid structure. From the literature review, it is visible that few studies have been reported for mixed convection in L-shaped lid-driven enclosures. The objective of this paper is to investigate the effect of Richardson number, Reynolds number, and Prandtl on mixed convection in a lid-driven L-shaped enclosure.

2. Problem Setup and Governing Equations

The configuration of the current work, illustrated in Figure 1, consists of a steady state, laminar and incompressible mixed convection flow inside an L-shaped lid-driven cavity. The upper wall moves from left to right with a constant velocity U_0 allowing the Newtonian fluid to enter the domain with a cold

temperature *Tc*. The left and the bottom wall of the cavity are maintained at a hot temperature *Th* , the isolated right-side wall is shown dashed, while a cold temperature *Tc* is imposed at the rest of the walls. The width and the height of the cavity are noted by W and H respectively with W=H. The thickness of the cavity is represented by L. The aspect ratio of the cavity is defined as AR = L/H. The Boussinesq approximation is applied to the fluid with constant physical properties.

Taking into account the above-mentioned assumptions, the non-dimensional governing equations for the continuity, momentum, and energy conservation are given as follows:

$$\frac{\partial \mathrm{U}}{\partial \mathrm{X}}+\frac{\partial \mathrm{V}}{\partial \mathrm{Y}}=0 \tag{1}$$

$$\mathrm{U}\frac{\partial \mathrm{U}}{\partial \mathrm{X}}+\mathrm{V}\frac{\partial \mathrm{U}}{\partial \mathrm{Y}}=-\frac{\partial P}{\partial \mathrm{X}}+\frac{1}{\mathrm{Re}}\left[\frac{\partial^2 \mathrm{U}}{\partial \mathrm{X}^2}+\frac{\partial^2 \mathrm{U}}{\partial \mathrm{Y}^2}\right] \tag{2}$$

$$\mathrm{U}\frac{\partial \mathrm{V}}{\partial \mathrm{X}}+\mathrm{V}\frac{\partial \mathrm{V}}{\partial \mathrm{Y}}=-\frac{\partial P}{\partial \mathrm{Y}}+\frac{1}{\mathrm{Re}}\left[\frac{\partial^2 \mathrm{V}}{\partial \mathrm{X}^2}+\frac{\partial^2 \mathrm{V}}{\partial \mathrm{Y}}\right]+\mathrm{Ri}\,\theta \tag{3}$$

$$\mathrm{U}\frac{\partial \theta}{\partial \mathrm{X}}+\mathrm{V}\frac{\partial \theta}{\partial \mathrm{Y}}=\frac{1}{\mathrm{Re}\,\mathrm{Pr}}\left[\frac{\partial^2 \theta}{\partial \mathrm{X}^2}+\frac{\partial^2 \theta}{\partial \mathrm{Y}^2}\right] \tag{4}$$

The non-dimensional variables used in the equations are considered as follows:

$$P=\frac{p-P_0}{\rho U_0^2}, V=\frac{v}{V_0}, X=\frac{x}{H}, Y=\frac{y}{H},\quad U=\frac{u}{U_0}, \theta=\frac{T-T_0}{\Delta T} \tag{5}$$

The governing non-dimensional parameters, Richardson, Reynolds and Prandtl numbers, are defined as follow:

$$Gr=\frac{g\beta(T_h-T_c)H^3}{\nu^2}, Ri=\frac{Gr}{Re^2}, Re=\frac{U_0 L}{\nu},\quad \mathrm{Pr}=\frac{\nu}{\alpha} \tag{6}$$

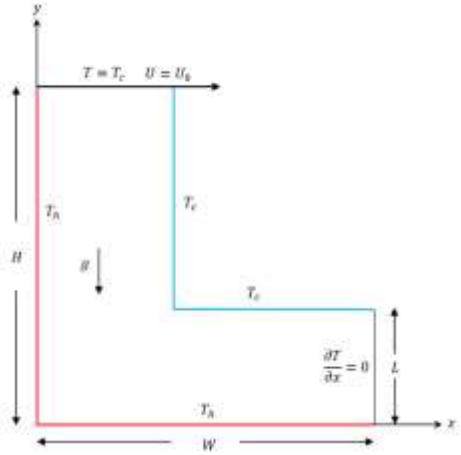

Figure 1: Physical configuration

The description of the problem is done by highlighting the boundary conditions, which can be expressed in their dimensionless form by:

$$\begin{aligned}
&X=0, U=V=0, \theta=1, 0\le Y\le 1\\
&Y=0, U=V=0, \theta=1, 0\le X\le 1\\
&X=1, \frac{\partial\theta}{\partial X}=0, 0\le Y\le L/H\\
&Y=L/H, U=V=0, \theta=0, L/H\le X\le 1\\
&X=L/H, U=V=0, \theta=0, L/H\le Y\le 1\\
&Y=1, \frac{\partial\theta}{\partial Y}=0, 0\le X\le L/H
\end{aligned} \tag{7}$$

In the current work, the stream function formulation is employed such that:

$$U=\frac{\partial \Psi}{\partial Y}, V=-\frac{\partial \Psi}{\partial Y} \tag{8}$$

Where Ψ is the dimensionless stream function, respectively, and is defined as:

$$\Psi=\frac{\psi}{U_0 H} \tag{9}$$

Local Nusselt number is defined to evaluate the heat transfer rate:

$$Nu_l=\left|\frac{\partial\theta}{\partial n}\right| \tag{10}$$

The average Nusselt number is obtained by integrating the local Nusselt number over the hot walls and is given by:

$$\overline{Nu}=\frac{1}{2H}\left(\int_0^W Nu_l\,\mathrm{d}X|_{Y=0}+\int_0^H Nu_l\,\mathrm{d}Y|_{X=0}\right) \tag{11}$$

3. Numerical Method and Validation of the Numerical Simulation

The finite volume method is used to resolve the previous formulations using the applied boundary conditions on the problem. Ansys/Fluent a solver based on the finite volume method, is adopted for numerical solutions.

The velocity-pressure coupling is handled by the SIMPLE algorithm, momentum and energy were computed using a second-order upwind procedure, while pressure was calculated using PRESTO. The convergence of the solution is obtained when the residuals of continuity, momentum, and energy equations reach 10^{-6}.

Table 1: Grid independency test at AR = 0.25, Ra = 10^5 and Pr = 0.71

Mesh	Number of nodes	Number of elements	$\overline{Nu}$	Error %
1	781	700	3.9314	-
2	1696	1575	3.8780	1.37
3	2961	2800	3.8589	0.49
4	**4576**	**4375**	**3.8499**	0.23
5	6541	6300	3.8449	0.13
6	8856	8575	3.8419	0.07

A grid resolution test is conducted to confirm the consistency and accuracy of this numerical investigation. The grid sensitivity is analyzed by evaluating the average Nusselt number at hot walls with different mesh resolutions, with AR = 0.25, Ra=10^4, Gr = 10^5 and Pr = 0.71; as illustrated in Table1. Increasing mesh resolution leads to a considerable decrease in the relative error, which indicates that the choice of mesh 4 (4576 nodes and 4375 elements) is reasonably accurate in terms of results as well as computational expense reduction.

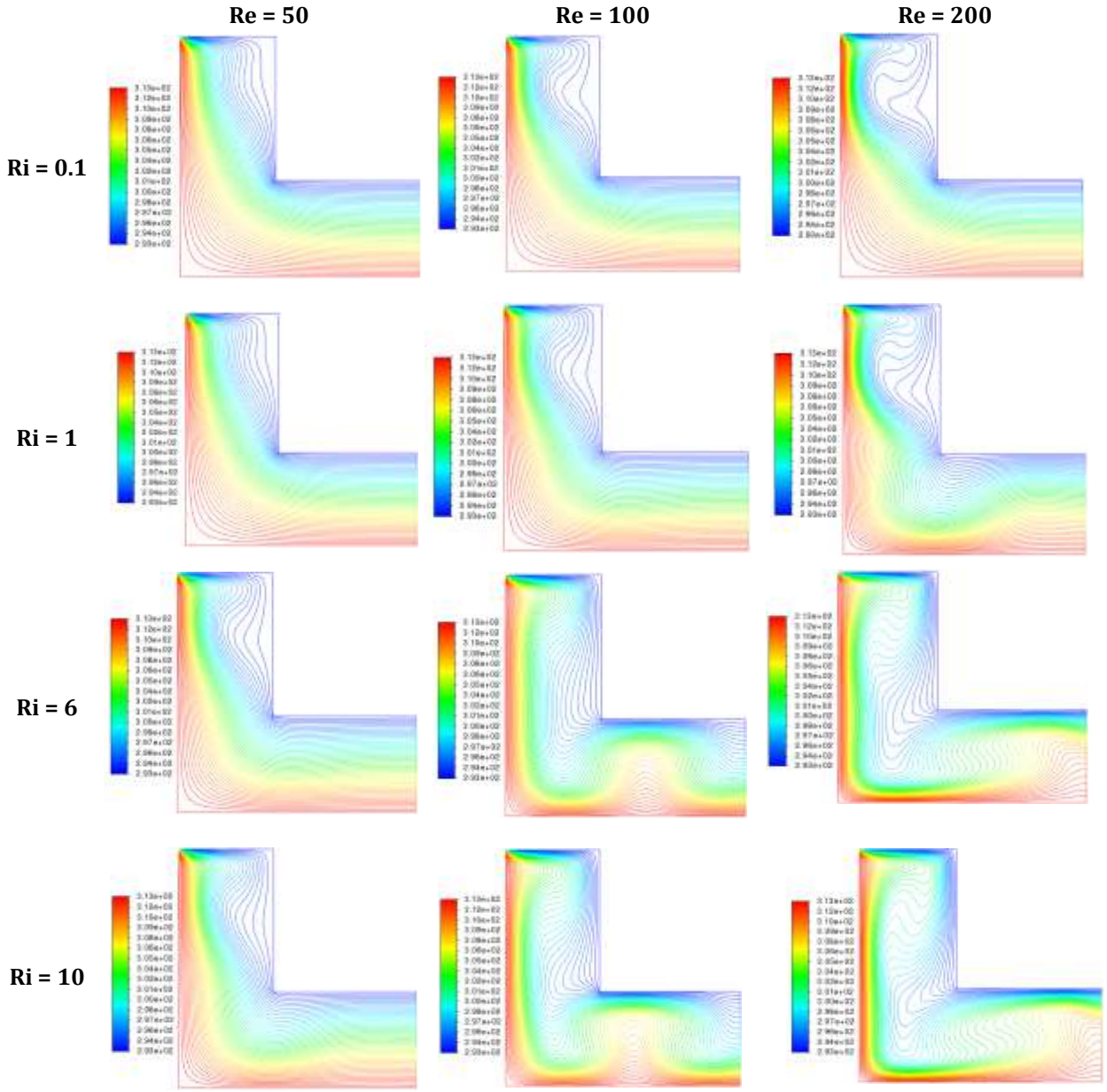

Figure 2: Variation of isotherms for different values of Richardson number and Reynolds number, while Pr = 0.71

In order to validate our model, we compared our results with those obtained by Sivakumar et al [8], Sharif [4], and Iwatsu et al [5] (Table 2) for a top-heated moving lid and bottom-cooled square cavity filled with air (Pr = 0.71).

We also compared our results for natural convection in a L-shaped cavity filled with air, with the results of Mahmoodi [2] and Tasnim and Mahmud [9] (Table3).

The comparisons presented in Table 2 and Table3, demonstrated good agreement between our results and the references.

4. Results and Discussion

The mixed convection phenomenon inside an L-shaped enclosure is influenced by several controlling parameters such as: Richardson number, Reynolds number and Prandtl number. Results are presented in forms of isotherm streamlines, and average Nusselt number.

The ranges are varied as 50≤Re≤200, 0.1≤Ri≤10, and 0.1 ≤ Pr ≤ 10 for an aspect ratio of AR = 0.4.

Table 2: Average Nusselt number *comparison with the literature for Re = 400, Gr = 10^4 and Pr = 0.71*

	Present	Sivakumar et al [8]	Sharif [4]	Iwatsu et al [5]
$\overline{Nu}$	**3.85**	3.85	3.82	3.62
Error%	-----	0%	0.78%	6.35%

Table 3: Average Nusselt number *comparison with the literature for B = 0.25, Ra = 10^4 and Ra = 10^5 and Pr = 0.71*

Ra	Present	Mahmoodi [2]	Tansim and Mahmud [15]
10^4	3.282	3.259	3.255
10^5	3.849	3.85	3.903

4.1 Effect of Richardson Number

As shown in Figure 2, isotherms were compared for different values of Richardson (Ri = 0.1, 1, 6, and 10) and Reynolds numbers (Re = 50, 100, 200) for Pr=0.71. For low Richardson numbers, a deformation of the isothermal lines can be observed near the inlet region of the enclosure. This deformation is due to the interaction between the imposed cold fluid entering the cavity and the hot wall. Thus, by increasing Reynolds number, the deformation of the isotherms is more pronounced. Apart from the inlet region, increasing Reynolds number for the lower value of Richardson number has no effect on the isotherms, which consists of stratified parallel lines to the non-adiabatic walls. The reason is that, in this case, the buoyancy forces are weakened, which leads to the domination of the conduction heat transfer mode.

For Ri = 1, it appears that isotherms form a smooth and stratified pattern along the hot and cold wall at the bottom right side of the cavity for Re<200. At Re = 200, a slight deformation of isotherms is observed at the right side of the cavity due to the increase of the convection phenomenon. For Ri=6 and 10, it can be observed that for a low value of Reynolds number (Re = 50), the effect of Richardson number is not significant. On the other hand, when increasing Reynolds number (Re = 100), an increase in isotherms distortion between the constant temperature walls is noticed with the formation of a single plume in form of fungi due to the stronger convective effect replacing the smoother conductive- dominated features.

Thus, increasing Reynolds number, because of the fixed high value of Richardson number, leads to the increase of the natural convection and the forced convection phenomenon. The latter can be noted for Re = 200 where the plume is carried to the right adiabatic wall which is due to the flow penetration through the narrow right side of the enclosure. Consequently, the isothermal lines are compressed against the constant-temperature walls, because of the high temperature gradient resulting from the increase in the buoyancy forces, which leads to the enhancement of heat transfer.

The streamlines are sketched in Figure 3 for different values of Richardson (Ri = 0.1, 1, 6, and 10) and Reynolds numbers (Re = 50, 100, 200). It can be seen that for the lowest value of the Richardson number, a small cell that rotates in the clockwise direction is formed near the inlet, which is due to the flow penetration from the upper side of the cavity. When increasing Richardson number (Ri =1) streamlines start bending towards the bottom in the vertical part of the cavity, where a large recirculation cell is generated and expends by increasing Reynolds number.

At higher values of Richardson number (Ri = 6), one single vortex can be depicted for Re = 50, while three vortices are generated for Re = 100. The bigger main vortex and the vortex near the right-side wall of the enclosure are clockwise, while the other vortex rotates in the counter-clockwise direction. The two cells in the narrow region of the cavity have features consistent with a Rayleigh-Benard natural convection cell, its emergence is due to the instable vertical buoyancy between the two non-adiabatic walls. With a further increase in the Reynolds number (Re = 200), the number of the rotating vortices decreases to two counter-rotating vortices. The reason is that when increasing Reynolds number, the flow penetrates deeper through the narrow right side of the cavity, which causes the two counter rotating cells to merge into a single big recirculation cell.

Figure 4 depicts vertical velocity component profile. The results were drawn for two different Reynolds values of Re = 50 and 200 and that for Ri numbers ranging from 0.1 to 10. Generally, it can be seen that the positive values in the first half of the velocity profile reflects the ascending fluid along the hot wall. For Re = 50, and for all the Richardson number values, the fluid in contact with the hot wall gets warmer, ascends with a positive velocity then turns in clock-wise direction, helped with the incoming inlet cold fluid, then descends along the cold wall with a negative velocity. For Re = 200, the profiles show the same trend as the other case. However, a slight deformation of the profiles is observed, which is due to the increase in the Reynolds number.

Comparing the two cases, the maximum velocity value in the former case is approximately 7 times more that the latter case. The reason for this is that increasing Reynolds number increases the size and the strength of the convective cell in the vertical part of the cavity, which increases its vertical velocity near the hot wall.

Figure 5 depicts the non-dimensional temperature profile for Re = 50 and 200 and that for Ri numbers ranging from 0.1 to 10. For the case of Re=50, it is seen that the temperature profiles demonstrate a quasi-linear behavior, which is due to the weakness of the vortex formed by the entering fluid. However, for the case the case of Re = 200, it can be observed that the profiles have a curvature which decreases by decreasing Richardson numbers.

Figure 6 represents the variation of the average Nusselt number on the hot wall for different Richardson numbers (Ri = 0.1, 1, 3, 6, 8, and 10), for Re = 50, 100, 150, and 200.

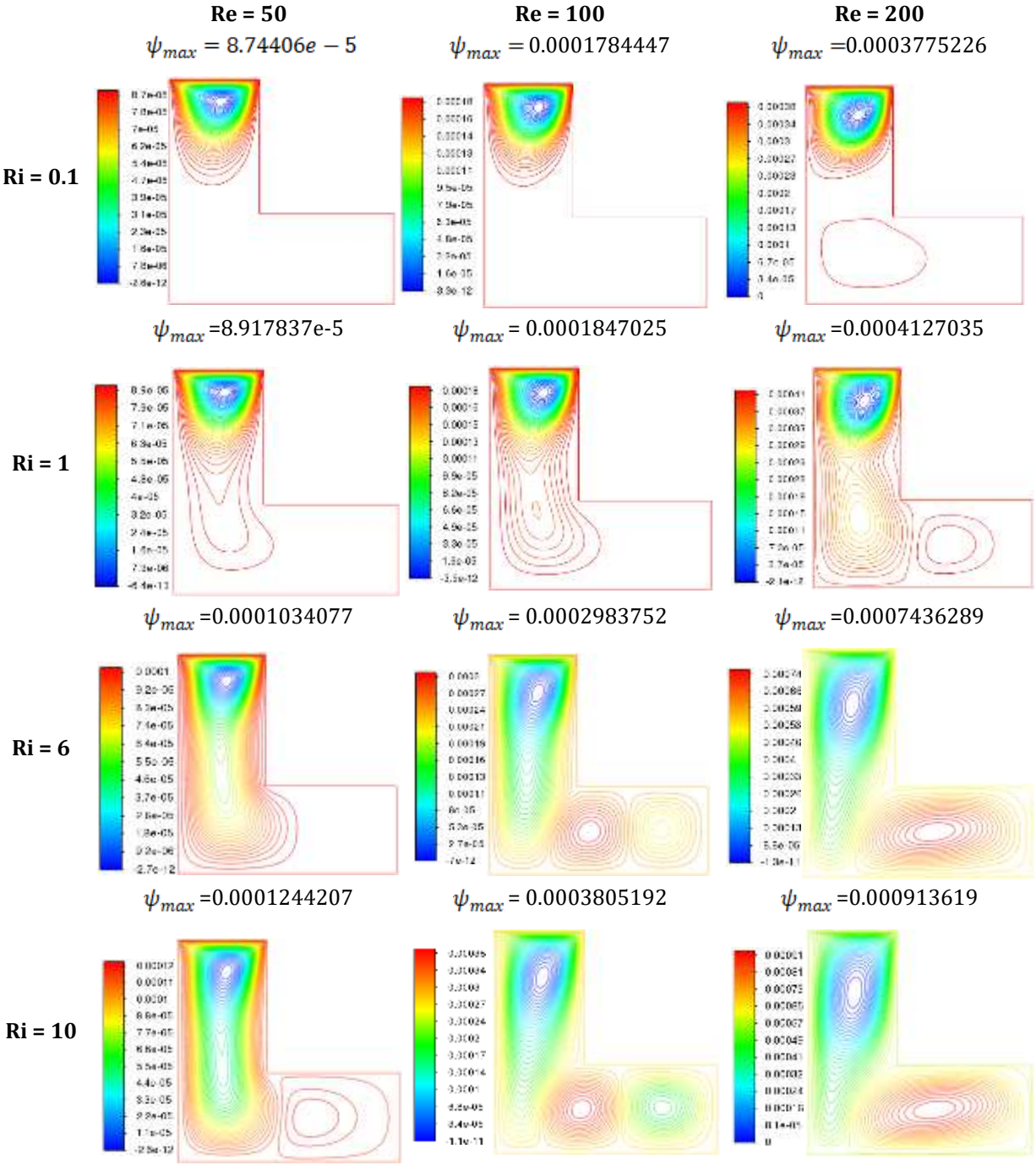

Figure 3: Variation of streamlines for different values of Richardson number and Reynolds number, while Pr = 0.71

A slight increase in the Nusselt number can be observed when varying Richardson number for Re=50, while a clear ascent is noted for the other values of Reynolds number (Re = 100, 150, and 200), Increasing Richardson number for a fixed value of Reynolds number leads to an increase in natural convection which strengthen the buoyancy forces.

As a result, the temperature gradient is increased which causes a noticeable increase in heat transfer rate.

4.2 Effect of Prandtl Number

Figure 7 shows the comparison of isotherms for different values of Prandtl numbers (Pr = 0.1, 1, 7, and 10) and Richardson numbers (Ri = 0.1, 1, and 10) for a fixed Reynolds number Re = 100. For Ri=0.1, it can be seen that for Pr = 0.1, temperature distribution is uniform and stratified in comparison with high Prandtl numbers (Pr > 1), where an increase in the curvature of the isotherms.

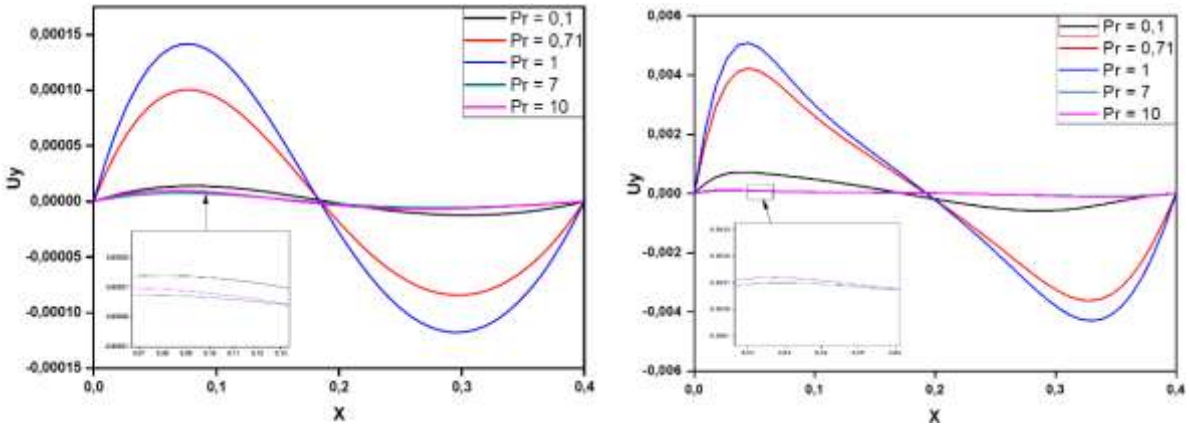

Figure 4: The distributions of the vertical velocity component at y = 0.5, Pr = 0.71, for different Richardson numbers at Re = 50 (left) and Re = 200 (right)

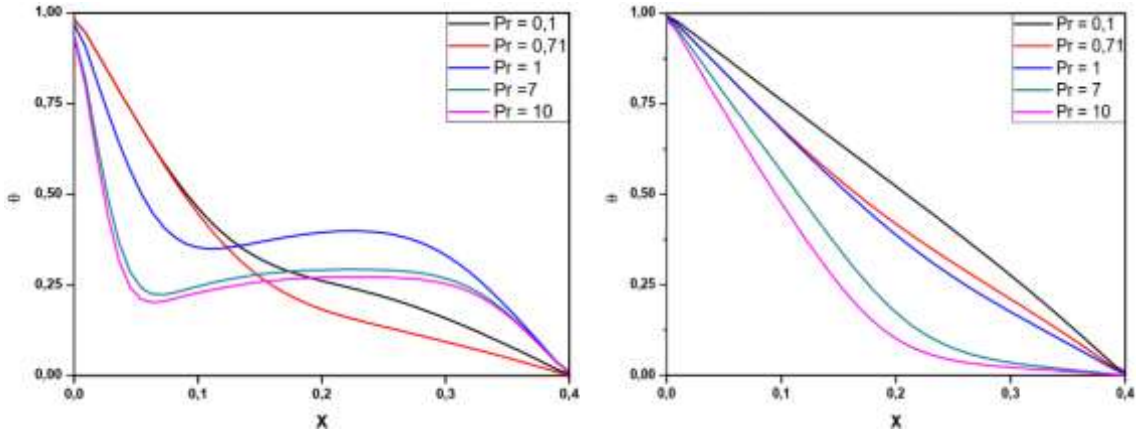

Figure 5: The distributions of the non-dimensional temperature and vertical velocity at y = 0.5, Pr = 0.71, for different Richardson numbers at Re = 50 (left) and Re = 200 (right)

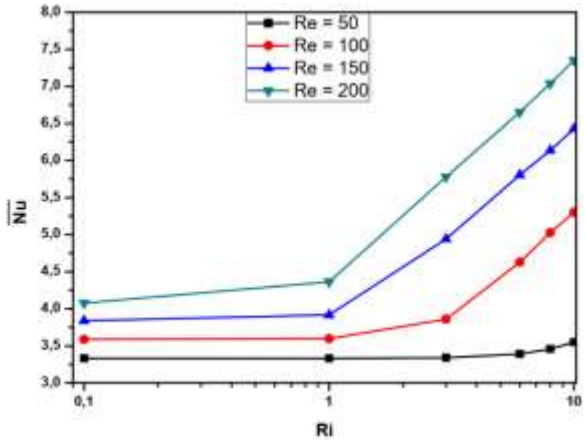

Figure 6: Distribution of the average Nusselt number along the heated walls as a function of Richardson number for Pr = 0.71 and different values of Reynolds numbers

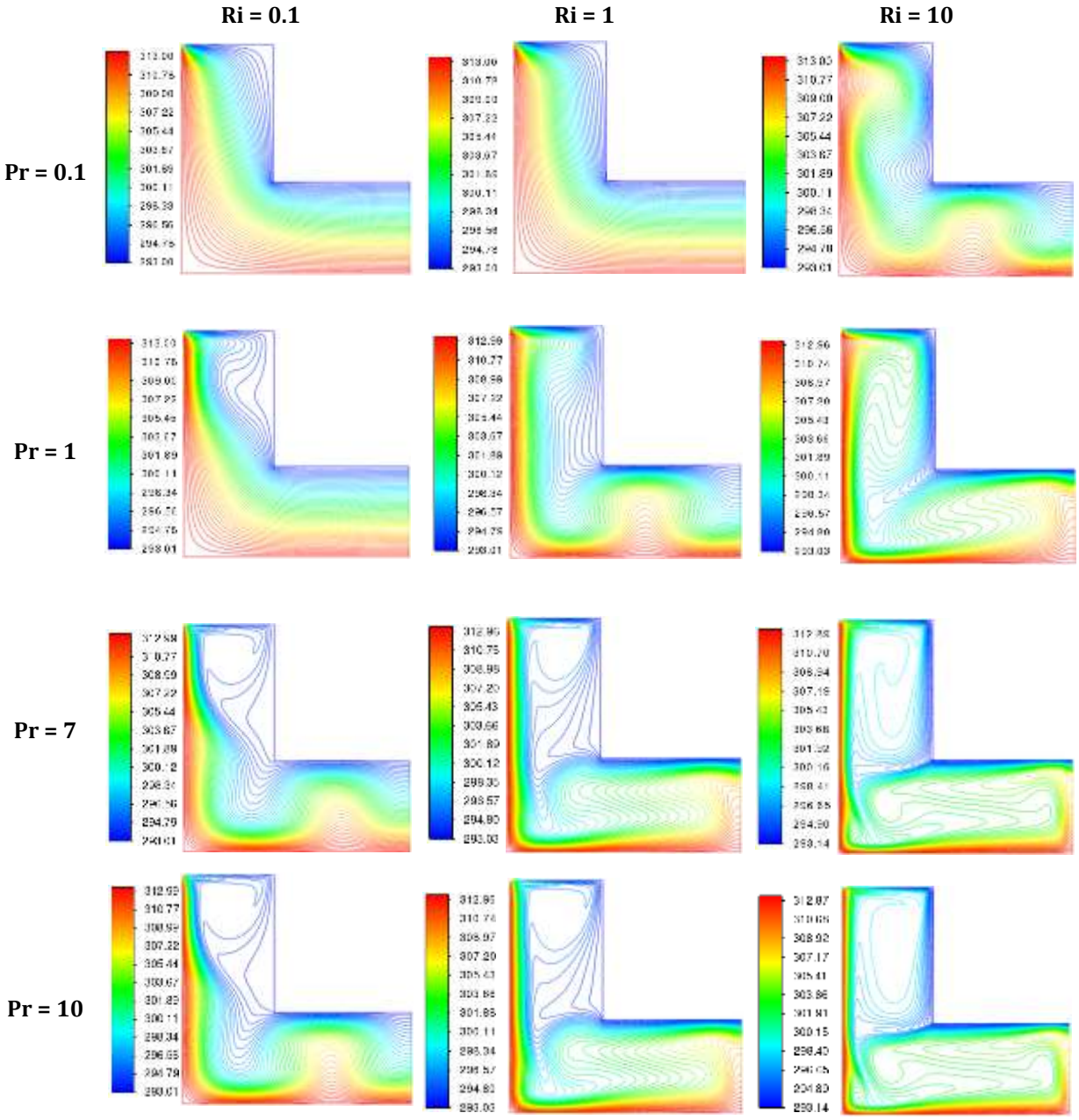

Figure 7: Variations of the isotherms for different values of Prandtl number and Richardson number, while Re = 100

The latter is due to the fact that high Prandtl number fluids are characterized by the domination of the momentum diffusivity over the thermal diffusivity, which leads to a much more effective convective heat transfer. Moreover, it can be seen that for Pr = 7 and 10, a thermal plume is formed in the narrow side of the enclosure, which is similar to the structures formed in the Rayleigh Bernard natural convection phenomenon, which indicates that, as the Prandtl number increases, the dominant heat transfer shifts from conduction to convection. We also note that, while increasing Richardson number for Pr = 0.1, there is no significant change is the isotherms except for the case where Ri = 10. On counterpart, for Pr ≥ 1, the distortion in the isotherms occurs for all the values of Richardson numbers. It is because high Prandtl numbers are characterized by a thin thermal boundary layer, which means that heat diffuses more slowly and consequently, the flow is much more affected by buoyancy forces and the fluid entering the enclosure from the inlet.

Figure 8 provides information about the influence of Prandtl number on streamlines for different Richardson numbers. For Ri = 0.1, we note the formation of a vortex rotating clockwise, near the inlet. It is caused by the cold fluid entering the enclosure, we also note that as Prandtl number increases, the vortex tends to grow in strength and size towards the bottom of the enclosure.

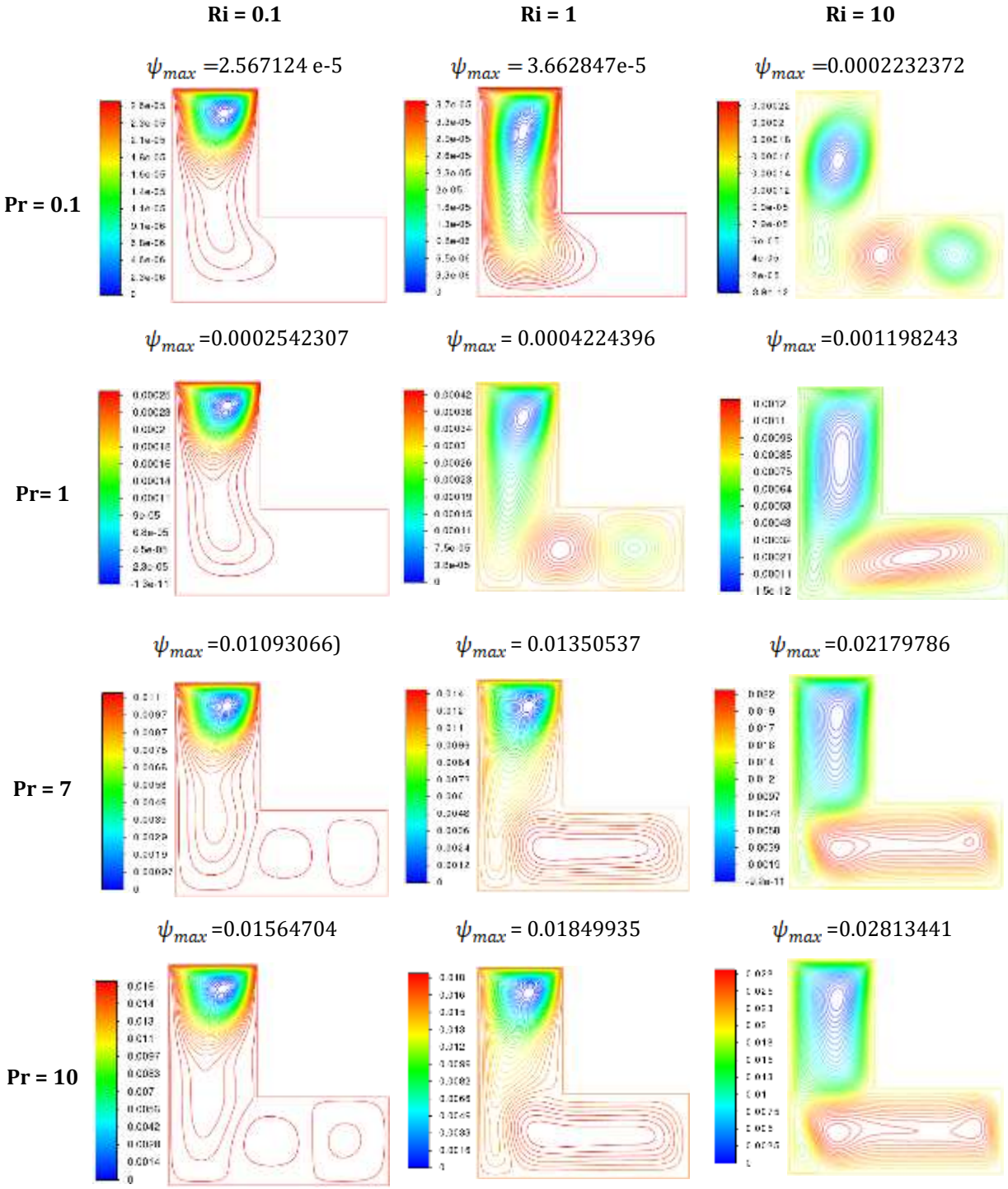

Figure 8: Variations of the streamlines for different values of Prandtl number and Richardson number, while Re = 100

We also note that, for Pr = 0.1 and while increasing Richardson number to unity, the vortex is strengthened and the fluid circulation tends to be stronger in the vertical side of the cavity. For Ri = 10, we notice a significant change in the streamlines, where three vortices are formed. The bigger main vortex is reduced by the two newly formed counter rotating vortices.

These vortices located on the right side of the cavity, are created by the strong buoyancy forces created by the increase of Richardson number. For Pr > 1, when Ri > 1, the two small vortices merge into on horizontal big vortex that rotates in the counter clockwise direction that occupies the whole horizontal part of the enclosure.

Furthermore, we also note that the maximum stream function value occurs for the highest Prandtl number case, at the highest Richardson number value, where the recirculation rate is at its highest.

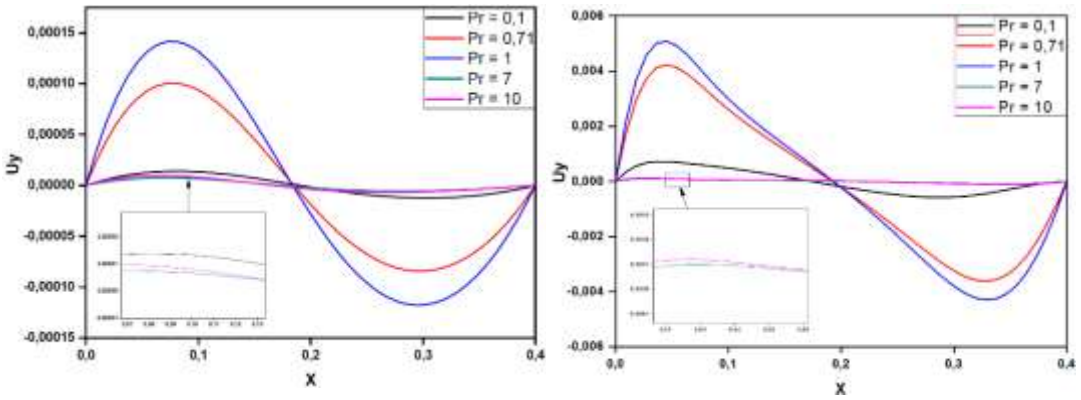

Figure 9: The distributions of the vertical velocity component at y = 0.5, Re = 100, for different Prandtl numbers at Ri = 0.1 (left) and Ri = 10 (right)

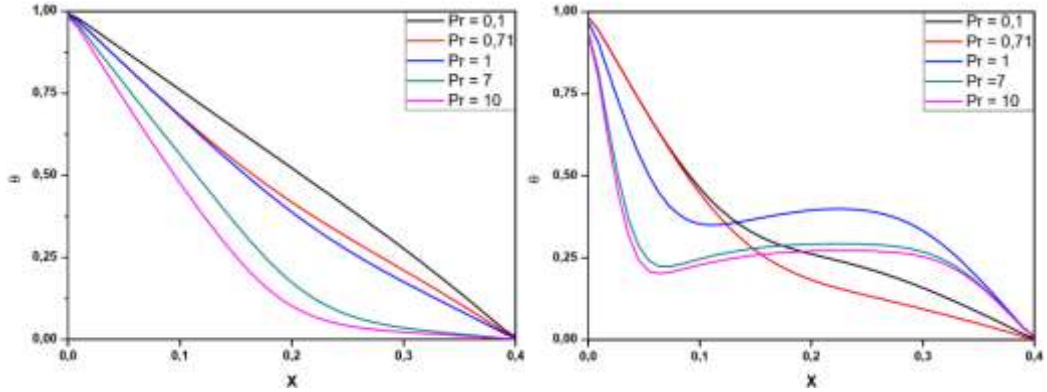

Figure 10: The distributions of the non-dimensional temperature profile at y = 0.5, Re = 100, for different Prandtl numbers at Ri = 0.1 (left) and Ri = 10 (right)

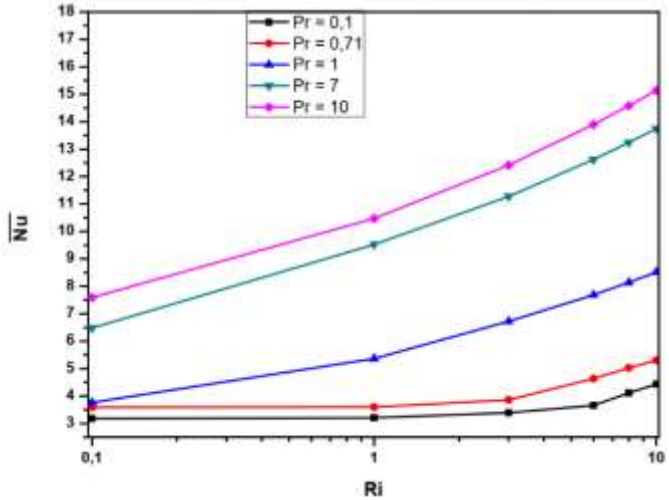

Figure 11: Distribution of the average Nusselt number along the heated walls at Re = 100 for different values of Pr and Ri

Figure 9 depicts vertical velocity component at y = 0.5, the results were drawn at a fixed Re = 100 for two different Richardson number values of Ri=0.1 and 10 and that for Prandtl numbers ranging from 0.1 to 10. Comparing the flow patterns for both Richardson number values Ri = 0.1 and 10, it is observed that the vertical velocities values of the latter case are approximately 10 times higher than the former case. It is due to the buoyancy forces that increases with the increase of the Richardson number, which give birth to strong convective flow and subsequently vertical velocities. The vertical velocity component values for Pr = 0.1 are lower than for Pr = 0.71 and 1, which can be explained by the fact that for low Prandtl numbers, thermal diffusivity is higher than momentum diffusivity which prioritize the heat diffusion and reduces temperature gradients and weakens the buoyancy forces. For higher Prandtl numbers (Pr = 7 and 10), the fluid's viscosity is high and therefore more

resistant to motion, which results on the inhibition of the convective currents and leads to lower vertical velocities.

The non-dimensional temperature profiles at y=0.5, for Ri = 0.1 and 10 and for the entire chosen range of Prandtl number are illustrated in Figure 10. It can be seen that the temperature profiles are more distorted for Ri = 10 compared to the case where Ri=0.1, this is due to the weakness of the convection regime, which is the consequence of the low value of the Richardson number.

The variation of the average Nusselt number for different Prandtl numbers along with Richardson numbers has been presented in Figure 11. It is seen that the average Nusselt number is the highest for the largest Prandtl number Pr = 10, and that for all values of Richardson number. This is due to the fact that the fluid with the highest Prandtl number can carry more heat away from the hot wall to the right side of the enclosure. On the other hand, the average Nusselt number slightly increases for lower values of Prandtl number and increases for higher Prandtl numbers (Pr > 0.71). The average Nusselt number increases clearly in the forced-dominated region (0.1≤ Ri ≤1), and increases slightly when increasing Richardson number.

5. Conclusions

A computational study was done to investigate the mixed convection inside an L-shaped cavity. Results are obtained for a wide range of Richardson numbers, Reynolds numbers, and Prandtl numbers. The following conclusions may be drawn from the present study:

- The mixed convection parameter Ri has a significant influence on temperature and flow field. Vortex numbers increase and a predominance of natural convection over forced convection is observed with increasing values of Richardson number. The average Nusselt number at the heated walls increases as Reynolds number and Richardson number increase.

- Increasing Reynolds number has a significant effect on the non-dimensional and velocity profiles, where the maximum velocity value is approximately 7 times more for the highest value of Reynolds number.

- The influence of Prandtl number on isotherms and streamlines is clear for different values of Richardson number. Increasing Prandtl number for the different values of Richardson number leads to an increase in the average Nusselt number.

References

[1] Sahraoui, N. M., Houat, S., Saidi, N. (2017). Simulation of mixed convection in a horizontal channel heated from below by the lattice Boltzmann method. *Eur. Phys. J. Appl. Phys*, 78, 34806. https://doi.org/10.1051/epjap/2017170046

[2] Sahraoui, N. M., Houat, S., El Ganaoui, M. (2020). Numerical investigation of low Prandtl number effect on mixed convection in a horizontal channel by the lattice Boltzmann method. *Heat Transfer Asian Research*, 49, 4528– 4542. https://doi.org/10.1002/htj.21839

[3] Qadan, H., Alkasasbeh, H., Yaseen, N., Sawalmeh, M. Z., ALKhalafat, S. (2019). A Theoretical Study of Steady MHD mixed convection heat transfer flow for a horizontal circular cylinder embedded in a micropolar Casson fluid with thermal radiation. *Journal of Computational Applied Mechanics*, 50, 165-173. https://doi.org/10.22059/jcamech.2019.278376.372

[4] Selimefendigil, F., Oztop, H,F. (2016). Mixed convection in a two-sided elastic walled and SiO2 nanofluid filled cavity with internal heat generation: Effects of inner rotating cylinder and nanoparticle's shape. *J. Molecular Liquids* 212, 509–516. https://doi.org/10.1016/j.molliq.2015.09.037

[5] Chamkha, A,J., Mudhaf, A,A. (2005). Unsteady heat and mass transfer from a rotating vertical cone with a magnetic field and heat generation or absorption effects. *Int. J. Therm. Sci*, 44, 267–276. https://doi.org/10.1016/j.ijthermalsci.2004.06.005

[6] Grosan, T., Revnic, C., Pop, I., Ingham D. (2009). Magnetic field and internal heat generation effects on the free convection in a rectangular cavity filled with a porous medium. Int. J. Heat Mass Transfer 52,1525–1533. https://doi.org/10.1016/j.ijheatmasstransfer.2008.08.011

[7] Shin, D.H., Kim, C.S., Park, G.C., Cho, H.K. (2017). Experimental analysis on mixed convection in reactor cavity cooling system of HTGR for hydrogen production. *Int. J. Hydrog. Energy*, 42 (34),22046–22053. https://doi.org/10.1016/j.ijhydene.2017.06.232

[8] Hayat, T., Shehzad, S.A., Qasim, M. (2011). Mixed convection flow of a micropolar fluid with radiation and chemical reaction. *Int. J. Numer. Methods Fluids*, 67 (11),1418 1436. https://doi.org/10.1002/fld.2424

[9] Rehman, S.U., Mir, N.A., Farooq, M., Rafiq, N., Ahmad, S. (2022). Analysis of thermally stratified radiative flow of Sutterby fluid with mixed convection. *Proceedings of the Institution of Mechanical Engineers, Part C: Journal of Mechanical Engineering Science*, 236 (2), 934 942. https://doi.org/10.1177/09544062211007887

[10] Harnby, N., Edwards, M.F., Nienow, A.W. (1997). Mixing in the process industries, second edition. Butterworth-Heinemann. https://doi.org/10.1016/B978-0-7506-3760-2.X5020-3

[11] Plankovskyy, S., Tsegelnyk, Y., Shypul, O., Romanova, T., Kombarov, V. (2024). Efficient Part's Shape and Its Placement in Closed Space under Thermal Energy Treatment. International *Journal of Mechatronics and Applied Mechanics*, 18,264-273. https://doi.org/10.17683/ijomam/issue18.31

[12] Rogovyi, A., Shudryk, O., Rezvaya, K., Stanciu, D.I, Petruniak, M., Bovkun, V., Ruzmetov, A. (2024). Features of Mathematical Modeling of Air Flow in the Paraxial Zone of a Vortex-Chamber Ejector with a Closed Outlet Channel. International *Journal of Mechatronics and Applied Mechanics*,18, 118- 125. https://doi.org/10.17683/ijomam/issue18.14

[13] Abdelmalek, N., Houat, S., Sahraoui, N. (2025). Numerical investigation of heat transfer in a partially open-ended enclosure containing heated body through the lattice Boltzmann method. *Journal of Mechatronics and Applied Mechanics*, 3846. https://doi.org/10.17683/ijomam/issue21.40

[14] Nayak, J., Agrawal, M., Mishra, S., Sahoo, S, S., Swain, R,K., Mishra, A. (2018). Combined heat loss analysis of trapezoidal shaped solar cooker cavity using computational approach. *Case Stud. Therm. Eng*, 12, 94-103. https://doi.org/10.1016/j.csite.2018.03.009

[15] Sharif, M. A. R. (2007). Laminar Mixed Convection in Shallow Inclined Driven Cavities with Hot Moving Lid on Top and Cooled from Bottom. *Applied Thermal Engineering*, 27, 1036–1042. https://doi.org/10.1016/j.applthermaleng.2006.07.035

[16] Iwatsu, R, R., Hyun, J. M., Kuwahara, K. (1993). Mixed Convection in a Driven Cavity with a Stable Vertical Temperature Gradient. *International Journal of Heat and Mass Transfer*, 36, 1601–1608. https://doi.org/10.1016/S0017-9310(05)80069-9

[17] Sivakumar, V., Sivasankaran, S. (2014). Mixed convection in an inclined lid-driven cavity with non-uniform heating on both sidewalls. *Journal of Applied Mechanics and Technical Physics*, 55, 634–649. https://doi.org/10.1134/S0021894414040105

[18] Dahani, Y., Hasnaoui, M., Amahmid, A., El Mansouri, A., Hasnaoui, S. (2020). Lattice Boltzmann simulation of combined effects of radiation and mixed convection in a lid-driven cavity with cooling and heating by sinusoidal temperature profile on one side. *Heat Transfer Engineering*, 41, 433-448. https://doi.org/10.1080/01457632.2018.1558009

[19] Papanicolaou, E., Jaluria, Y., (1991). Mixed convection from an isolated heat source in a rectangular enclosure. *Numerical Heat Transfer, Part A: Applications: An International Journal of Computation and Methodology*, 18:4, 427-461. https://doi.org/10.1080/10407789008944802

[20] Basak, E., Roy, S., Sharma, P, K., Pop, I. (2009). Analysis of mixed convection flows within a square cavity with linearly heated side wall(s). *Int. J. Heat Mass Transfer* 52 , 2224–2242. https://doi.org/10.1016/j.ijheatmasstransfer.2008.10.033

[21] Islam, A, W., Sharif, M, A, R., Carslon, E, S. (2012). Mixed convection in a lid driven square cavity with an isothermally heated square blockage inside. Int. J. Heat Mass Transfer 55, 5244–5255. https://doi.org/10.1016/j.ijheatmasstransfer.2012.05.032

[22] Ajmera, S, K., Mathur, A, N. (2015). Combined Free and Forced Convection in an Enclosure with different Ventilation Arrangements. *Procedia Engineering*, 127, 1173-1180. https://doi.org/10.1016/j.proeng.2015.11.456.

[23] Mohamad, A, A., Viskanta, R. (1991). Transient low Prandtl number fluid convection in a lid-driven cavity. *Numerical Heat Transfer, Part A: Applications: An International Journal of Computation and Methodology*,19:2, 187-205. https://doi.org/10.1080/10407789108944845

[24] Ruiz, R., Sparrow, E. M. (1987). Natural convection in V-shaped and L-shaped corners. *International Journal of Heat and Mass Transfer*, 30, 2539. https://doi.org/10.1016/0017-9310(87)90135-9

[25] Mahmoodi, M., (2011). Numerical simulation of free convection of a nanofluid in L-shaped cavities. *International Journal of Thermal Sciences*, 50, 1731. https://doi.org/10.1016/j.ijthermalsci.2011.04.009

[26] Kalteh, M., Hasani, H. (2014). Lattice Boltzmann simulation of nanofluid free convection heat transfer in an L-shaped enclosure. *Superlattices and Microstructures*, 66, 112. https://doi.org/10.1016/j.spmi.2013.12.004

[27] Shahid, H., Khan, W.A., Yaqoob, I. (2022). Natural convection in an L-shaped enclosure using multi-relaxation time lattice Boltzmann method. *Indian Journal of Physics*, 96, 2921–2939. https://doi.org/10.1007/s12648-021-02222-x

[28] Mohammadifar, H., Sajjadi, H., Rahnama, M., Jafari, S., Wang, Y. (2021). Investigation of Nanofluid Natural Convection Heat Transfer in Open Ended L-shaped Cavities utilizing LBM. *Journal of Applied and Computational Mechanics*, 7, 2064-2083. https://doi.org/10.22055/jacm.2020.33495.2235

[29] Armaghani, T., Sadeghi, M.S., Rashad, A.M., Mansour, M.A., Chamkha, A. J., Dogonchi, A.S., Nabwey, H.A. (2021). MHD mixed convection of localized heat source/sink in an Al2O3-Cu/water hybrid nanofluid in L-shaped cavity. *Alexandria Engineering Journal* ,60 (3), 2947–2962. https://doi.org/10.1016/j.aej.2021.01.031

[30] Naseri, N, S., Rabiei, F., Rashidi, M.M., Kwang, T.M. (2020). Lattice Boltzmann simulation of natural convection heat transfer of a nanofluid in a L-shape enclosure with a baffle. *Results in Physics* (19), 103413. https://doi.org/10.1016/j.rinp.2020.103413

[31] Tasnim, S, H., Mahmud, S. (2006). Laminar free convection inside an inclined L-shaped enclosure. *International Communications in Heat and Mass Transfer*, 33, 936-942. https://doi.org/10.1016/j.icheatmasstransfer.2006.05.008

[32] Ahmed, S, E., Mansour, M,A., Alwatban, A,M., Aly, A,M. (2020). Finite element simulation for MHD ferro-convective flow in an inclined double-lid driven L-shaped enclosure with heated corners. *Alexandria Eng. J*, 59 (1) , 217–226. https://doi.org/10.1016/j.aej.2019.12.026

[33] Sourtiji, E., Hosseinizadeh, S, F. (2012). Heat transfer augmentation of magnetohydrodynamics natural convection in L-shaped cavities utilizing nanofluids. *Therm. Sci*, 16, 489-501. https://doi.org/10.2298/TSCI1202489S

[34] Zhang, P., Ashraf, M.A., Liu, Z., Peng, W, X., Ross, D. (2020). The coupled lattice Boltzmann simulation of free convection in a finned L-shaped cavity filled with nanofluid. *International Journal of Numerical Methods for Heat & Fluid Flow*, 30 (3), 1478-1496. https://doi.org/10.1108/HFF-08-2019-0632

[35] Selimefendigil, F., Oztop, H, F. (2019). MHD mixed convection of nanofluid in a flexible walled inclined lid driven L-shaped cavity under the effect of internal heat generation. *Phys. Stat. Mech. Appl*, 534, 122144. https://doi.org/10.1016/j.physa.2019.122144

[36] Yeasmin, S., Billah, M, M., Molla, M, Z., Hoque, K, E. (2022). Numerical analysis of unsteady mixed convection heat transfer characteristics of nanofluids confined within a porous lid-driven L-shaped cavity. *Int. J. Thermofluids*, 16, 100218. https://doi.org/10.1016/j.ijft.2022.100218